Draft version October 18, 2019
Preprint typeset using LaTeX style emulateapj v. 12/16/11



# NEAR-INFRARED IMAGING OF A SPIRAL IN THE CQ TAU DISK

Taichi Uyama[1,2,3], Takayuki Muto[4], Dimitri Mawet[5,6], Valentin Christiaens[7], Jun Hashimoto[8,9,10], Tomoyuki Kudo[9], Masayuki Kuzuhara[8], Garreth Ruane[6], Charles Beichman[1,2], Olivier Absil[11], Eiji Akiyama[12], Jaehan Bae[13], Michael Bottom[6], Elodie Choquet[5], Thayne Currie[14,9,15], Ruobing Dong[16], Katherine B. Follette[17], Misato Fukagawa[3], Greta Guidi[18], Elsa Huby[19], Jungmi Kwon[20], Satoshi Mayama[21], Tiffany Meshkat[1], Maddalena Reggiani[22], Luca Ricci[23], Eugene Serabyn[6], Motohide Tamura[20,8,3], Leonardo Testi[24], Nicole Wallack[25], Jonathan Williams[26], and Zhaohuan Zhu[27]

*Draft version October 18, 2019*

## ABSTRACT

We present $L'$-band Keck/NIRC2 imaging and $H$-band Subaru/AO188+HiCIAO polarimetric observations of CQ Tau disk with a new spiral arm. Apart from the spiral feature our observations could not detect any companion candidates. We traced the spiral feature from the $r^2$-scaled HiCIAO polarimetric intensity image and the fitted result is used for forward modeling to reproduce the ADI-reduced NIRC2 image. We estimated the original surface brightness after throughput correction in $L'$-band to be $\sim 126$ mJy/arcsec$^2$ at most. The NIRC2 data correspond to an unexpectedly bright spiral that cannot simply be reproduced by scattered light, which suggests a hot spiral induced by a possible unseen protoplanet in the disk.

[1] Infrared Processing and Analysis Center, California Institute of Technology, 1200 E. California Blvd., Pasadena, CA 91125, USA
[2] NASA Exoplanet Science Institute
[3] National Astronomical Observatory of Japan, 2-21-1 Osawa, Mitaka, Tokyo 181-8588, Japan
[4] Division of Liberal Arts, Kogakuin University, 1-24-2, Nishi-Shinjuku, Shinjuku-ku, Tokyo, 163-8677, Japan
[5] Department of Astronomy, California Institute of Technology, 1200 E. California Blvd., Pasadena, CA 91125, USA
[6] Jet Propulsion Laboratory, California Institute of Technology, 4800 Oak Grove Dr., Pasadena, CA, 91109, USA
[7] Monash Centre for Astrophysics (MoCA) and School of Physics and Astronomy, Monash University, Clayton Vic 3800, Australia
[8] Astrobiology Center, National Institutes of Natural Sciences, 2-21-1 Osawa, Mitaka, Tokyo 181-8588, Japan
[9] Subaru Telescope, National Astronomical Observatory of Japan, Mitaka, Tokyo, 181-8588, Japan
[10] Department of Astronomy, School of Science, Graduate University for Advanced Studies (SOKENDAI), Mitaka, Tokyo 181-8588, Japan
[11] Space Sciences, Technologies, and Astrophysics Research (STAR) Institute, Université de Liège, Liège, Belgium
[12] Institute for the Advancement of Higher Education, Hokkaido University, Kita17, Nishi8, Kita-ku, Sapporo, 060-0817, Japan
[13] Department of Terrestrial Magnetism, Carnegie Institution for Science, 5241 Broad Branch Road NW, Washington, DC 20015, USA
[14] NASA-Ames Research Center, Moffett Field, CA, USA
[15] Eureka Scientific, 2452 Delmer Street Suite 100, Oakland, CA, USA
[16] Department of Physics & Astronomy, University of Victoria, Victoria, BC, V8P 1A1, Canada
[17] Physics and Astronomy Department, Amherst College, 21 Merrill Science Drive, Amherst, MA 01002, USA
[18] ETH Zurich, Institute for Particle Physics and Astrophysics, Wolfgang-Pauli-Str. 27, 8093 Zurich, Switzerland
[19] LESIA, Observatoire de Paris, Université PSL, CNRS, Sorbonne Université, Univ. Paris Diderot, Sorbonne Paris Cité ,5 place Jules Janssen, 92195 Meudon, France
[20] Department of Astronomy, The University of Tokyo, 7-3-1, Hongo, Bunkyo-ku, Tokyo 113-0033, Japan
[21] The Graduate University for Advanced Studies, SOKENDAI, Shonan International Village, Hayama-cho, Miura-gun, Kanagawa 240-0193, Japan
[22] Institute of Astrophysics, KU Leuven, Celestijnlaan 200D, 3001 Leuven, Belgium
[23] Department of Physics and Astronomy, California State University Northridge, 18111 Nordhoff Street, Northridge, CA 91330, USA
[24] ESO/European Southern Observatory, Karl-Schwarzschild-Strasse 2, 85748 Garching bei Mnchen, Germany
[25] Division of Geological and Planetary Sciences, California Institute of Technology, 1200 E. California Blvd., Pasadena, CA 91125, USA
[26] Institute for Astronomy, University of Hawaii, Honolulu, HI 96822, USA
[27] Department of Physics and Astronomy, University of Nevada, Las Vegas, 4505 S. Maryland Pkwy, Las Vegas, NV, 89154-4002

## 1. INTRODUCTION

Protoplanetary disks are good laboratories for understanding the relationship between planet formation and disk evolution mechanisms. Previous photometric/spectroscopic studies of young stellar objects (YSOs) with infrared (IR) excesses predicted gaps in their disks (transitional disk; Strom et al. 1989). As instruments have developed, high-spatial resolution observations with near-IR polarimetric imaging or (sub-)mm interferometry revealed more asymmetric disks with gaps (e.g., Hashimoto et al. 2012), rings (e.g., ALMA Partnership et al. 2015), spirals (e.g., Muto et al. 2012; Benisty et al. 2015; Pérez et al. 2016), dust traps (e.g., van der Marel et al. 2013) and velocity kink in gas kinematics (e.g., Pinte et al. 2018). Polarization differential imaging (PDI; Kuhn et al. 2001) observations provide polarimetric intensity (PI), which traces scattered starlight from the disk surface. On the other hand, radio continuum observations measure thermal emission of dust grains in the disk midplane and those at particular frequency windows can probe the distribution of different layers of molecular gas species. Performing interferometric observation in radio wavelength enables to achieve sufficient spatial resolution to resolve detailed asymmetric structure. These morphologies motivated detailed investigations of disk evolution mechanisms.

In particular, spiral arms are one of the most intriguing signposts of planet formation in the disk because a protoplanet behaves as a perturber of the disk, which can lead to spiral formation (Zhu et al. 2015; Dong et al. 2018a), but yet no confirmed connection between an observed spiral arm and a planetary mass companion has been made observationally (but see Wagner et al. 2019). Gravitational instability in the disk can produce spirals (Dong et al. 2015a). High contrast imaging searches for young planets, in parallel to disk studies, have not successfully detected dthe most convincing protoplanets within such disks until PDS 70b was reported recently (Keppler et al. 2018). The results of that paper support the theory that planets really form in protoplanetary disks. In the near future one can expect to discover more planets undergoing formation and further searches for asymmetric disk features as well as for protoplanets will help to understand the links between planet formation and disk evolution.

CQ Tau (RA = 05:35:58.47, Dec = +24:44:54.1) is a YSO in the Taurus star forming region (F2-type, $1.67 M_{\odot}$, ∼10 Myr, 162 pc; Natta et al. 2001; Gaia Collaboration et al. 2018; Ubeira Gabellini et al. 2019). Carbon investigation for CQ Tau suggested that it is likely a transitional disk (Chapillon et al. 2010). An ALMA observation reported a large gap in the 1.3-mm continuum, $^{13}$CO, and $^{18}$CO (Ubeira Gabellini et al. 2019). The gap sizes in the dust and gas are estimated at 56 au and 20 au, respectively. Ubeira Gabellini et al. (2019) also performed a 3D numerical simulations and suggested an unseen protoplanet in the disk. To further search for protoplanets as well as asymmetric features in the CQ Tau disk, we used two high-contrast imaging observations with Keck/NIRC2 and Subaru/AO188+HiCIAO. Although we did not detect any companion candidates, we detected a spiral feature in the disk. In this study, we analyze the detected spiral feature and investigate the possible links to ongoing planet formation.

## 2. OBSERVATIONS AND RESULTS

We used two infrared data sets taken from Keck/NIRC2 and Subaru/AO188+HiCIAO. We also used an ALMA archival image, observed in Cycle 5 (ID: 2017.1.01404.S, PI: L. Testi), which achieved a noise level of ∼23 $\mu$Jy/beam and a beam size of 69 mas and 51 mas for major-axis and minor-axis, respectively, for comparison with the infrared data. Details of this data set as well as other ALMA data of CQ Tau are described in Ubeira Gabellini et al. (2019). Table 1 summarizes observing logs for both observations. Sections 2.1 and 2.2 describe each observation and its result. Section 2.3 compares both results.

### 2.1. *Keck/NIRC2*

CQ Tau was observed on UT 2018 Dec 24 (PI: D. Mawet) using the Keck/NIRC2 vortex coronagraph (Mawet et al. 2017; Serabyn et al. 2017; Xuan et al. 2018) combined with angular differential imaging (ADI; Marois et al. 2008). The observation achieved angular rotation of ∼111°. No standard stars were taken in the same epoch and we did not conduct PSF subtraction by reference differential imaging (RDI; Ruane et al. 2019) in this study. We measured the off-axis PSF and determined that the full width at half maximum (FWHM) was 9.2 pix (∼0.″0915 with a pixel scale of 9.972 mas/pix). After a first reduction including flat fielding, bad-pixel correction, sky-subtraction, and image registration, the data set was processed via the vortex image processing (VIP; Gomez Gonzalez et al. 2017)[28] package that applies principal component analysis (PCA) for the ADI reduction (Amara & Quanz 2012; Soummer et al. 2012).

Figure 1 shows the Keck/NIRC2 ADI-reduced image of CQ Tau overlaid with the ALMA continuum (left) and Subaru/HiCIAO PI (right; see Section 2.2 for the data). We adopted principal component (PC)=8 for presenting our result because this image shows an extended object at separations between ∼0.″2 and 0.″4, and position angles (PAs) between ∼45° and 110° with signal-to-noise ratio (SNR)∼7–8. The feature appears robust because it survives for a wide range of PC values, as shown in Appendix A. We marginally found some other sources (see Figure 7) in a set of ADI-reduced images, whose SNRs fall less than 5 at a certain PC and do not discuss other companion candidates. We converted ADU into the surface brightness using a previous $L'$-band photometry (2.4 Jy for CQ Tau; McDonald et al. 2017) and the brightest region in this feature has 68±8.5 mJy/arcsec$^2$. The VIP package enables to set different fields of view (FoV) and inner working angle (IWA). We adopted IWA=16 pix so that the asymmetric feature is reproduced with a higher SNR. We checked the ADI-reduced image with smaller IWA to check whether other companion candidates appear at inner separations and confirmed that there showed residuals of speckles that vary among different PCs. We attempted to fit this signal with a point-source Gaussian, which provided a poor match and thus we concluded that it corresponds to an asymmetric structure in the CQ Tau disk.

[28] https://github.com/vortex-exoplanet

**Table 1**
Observing logs

| Instrument | Date (*UT*) | Observing Mode | Band | Total Exposure Time [sec] |
|---|---|---|---|---|
| Keck/NIRC2 | 2018 December 24 | ADI | $L'$ | 1800 |
| Subaru/HiCIAO | 2015 December 31 | PDI[a] | $H$ | 540 |

[a]ADI was combined with PDI but we focus on only PDI reduction in this study (see Section 2.2).

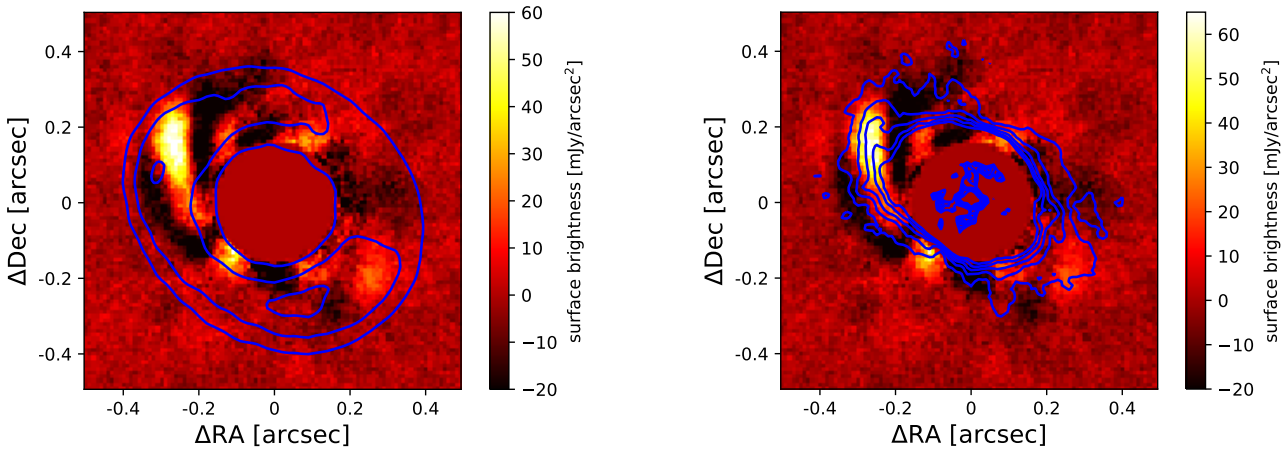


**Figure 1.** (left) Keck/NIRC2 $L'$-band image of CQ Tau overlaid with contours of the ALMA dust continuum image at 1.3 mm at 30, 50, and 70$\sigma$ (1$\sigma$ =23 $\mu$Jy/beam), respectively (blue). The central star is masked by the algorithm. North is up and East is left. The color scale shows surface brightness in mJy/arcsec$^2$ unit. (right) Same as the left figure except for the contours. The contours correspond to Subaru/HiCIAO $H$-band PI data at 10, 20, 30, 40, and 50 mJy/arcsec$^2$, respectively (blue).

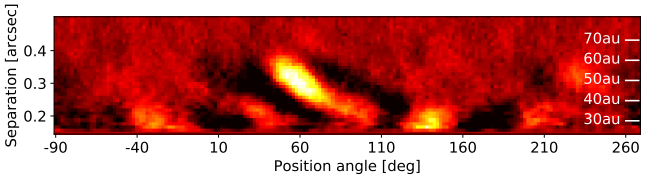


**Figure 2.** Polar-projected image of the NIRC2 image in Figure 1. We arrange the image starting at a position angle of -90° to show the spiral feature clearly.

Figure 2 shows a polar-projected image suggesting that this feature likely corresponds to a spiral. CQ Tau is one of only a few systems that have a spiral detected in $L'$-band (e.g., HD 100546 and MWC 758; Currie et al. 2015; Reggiani et al. 2018). We then compared our results with the ALMA archival data. The spiral overlaps with the ring of dust continuum, but the ADI-reduced signal experiences self-subtraction by the reduction algorithm as negative regions shown at both sides of the spiral. Centrosymmetric features in the CQ Tau disk will also be removed by self-subtraction and thus will not be seen in the ADI-reduced image (Milli et al. 2012).

Apart from the spiral feature, we did not detect any companion candidates within $\sim$0.″9 from the central star. The NIRC2 figure with a larger field of view (FoV) is shown in Appendix A. We then calculated noise profiles as a function of separation relative to the signal from the central star. Figure 3 shows a 5$\sigma$ detection limit of the NIRC2 data. Although the spiral feature affects the detection limit between $0.''2-0.''4$, we achieved $2.9\times10^{-5}$ at 0.″5. Compared with an evolutionary model (COND03; Baraffe et al. 2003) assuming 10 Myr, our contrast limit could constrain down to $\sim$5 $M_{\rm J}$ outside the spiral.

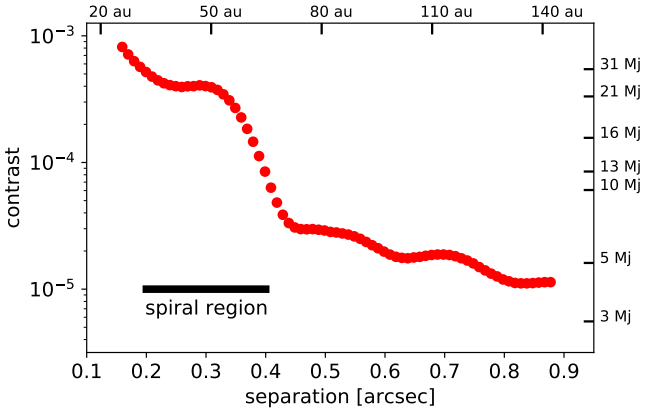


**Figure 3.** 5$\sigma$ contrast limit of the NIRC2 image with PC=8. We also plot expected contrast of substellar-mass object on the right using the COND03 model.

### 2.2. *Subaru/HiCIAO*

Subaru/AO188+HiCIAO observed CQ Tau in a combination of PDI and ADI as part of the SEEDS project (Tamura 2009). No coronagraph was used in this observation. The total exposure time of the HiCIAO data is only 9 min with FWHM=5.3 pix ($\sim$50 mas with a pixel scale of 9.5 mas/pix), which achieved an inner working angle of $\sim$ 0.″77 after the ADI reduction and is insufficient for searching planets embedded in the CQ Tau disk (for the ADI result at separations $\geq 1.''0$, see Uyama et al. 2017). In this study, we focus only on the PDI reduction. SEEDS adopted standard PDI (sPDI) and quad PDI (qPDI), where a different number of Wollaston prisms was used, and sPDI was applied to CQ Tau's observation (for detailed information see Uyama et al.

2017). After the first reduction of destriping the HiCIAO pattern, flat fielding, distortion correction, and image registration, we reduced the polarimetric data sets by means of an `IRAF` pipeline[29], which was used in previous HiCIAO PDI studies (e.g., Hashimoto et al. 2011, 2012). Figure 4 shows the PI image of CQ Tau overlaid with ALMA continuum. The whole disk cannot be investigated since there are residual speckles that cannot be removed through post-processing due to short exposure time. We did not detect a gap in the surface of CQ Tau's disk. The PI image shows the spiral feature at the same location as shown in the NIRC2 image. In order to investigate the SNR of the spiral, we used perpendicular regions to the spiral whose PAs range 125°-165°, 305°-345° for calculating a noise (defined as standard deviation in the specified area) radial profile. We finally confirmed that the spiral has an SNR$\sim$5–6 in the PI image. There may be other disk features shown in the PDI-reduced image but below $5\sigma$ significance due to speckles in the inner region. An $r^2$-scaled PI image (see Figure 5 for a polar-projected image) clearly shows the spiral feature. There is another extended region at PAs between 10° and 90°, which is perhaps another asymmetric feature and possibly detected in the NIRC2 data with PC=5, 8, and 10 in Figure 7 with insufficient significance. We discuss this inner feature in Section 2.3. We note that a gap-like feature close to the central star may be affected by $r^2$-scaling because the original HiCIAO data set does not show such a feature (see the left image in Figure 4 for the PI signal and the right image in Figure 1 for the contour).

### 2.3. *Comparison of the Two Data Sets*

In both observations we clearly detected the spiral feature, which overlaps with the ring structure in the millimeter continuum detected by ALMA. The presence of the spiral is consistent with a prediction of $\sim$6–9 $M_J$ planet at 20 au (Ubeira Gabellini et al. 2019). However, our observation could not achieve a sufficient contrast limit to detect/constrain such a faint protoplanet. We checked whether a counterpart of the spiral is shown in the ALMA gas data. Tang et al. (2017) reported a pair of spirals for AB Aur at $^{12}$CO emission that correspond to the PI signal (Hashimoto et al. 2011). However, Ubeira Gabellini et al. (2019) did not show any clear spiral features in the $^{12}$CO data.

The right image in Figure 1 compares the NIRC2 and HiCIAO results and these shapes show a good agreement with each other. Polar-projected images (Figures 2 and 5) also clearly show a spiral feature in both cases. We note that the surface brightness in each band shows a different parameter. The NIRC2 and HiCIAO results correspond to total intensity and polarimetric intensity, respectively. We discuss the difference between these results in Section 3.1. We measured the pitch angle based on the best-fit logarithmic spiral to the trace of the spiral. The trace was identified as radial maxima in azimuthal bins of 1° in the image obtained after deprojection using inclination and position angle of the major axis derived by Ubeira Gabellini et al. (2019): $i = 35°$ and $\mathrm{PA}_a = 55°$. Since the spiral feature in the NIRC2 image experiences self-subtraction and is distorted by the reduction algorithm, we used only the HiCIAO data to measure the pitch angle. The PI data corresponds to scattering profiles from the disk surface and does not experience self-subtraction. The fitted result for the spiral (the central image in Figure 4) is $34° \pm 2°$. We also attempted to fit the extended inner region at PAs between 10° and 90°. The result is shown in the right image of Figure 4 and the pitch angle is measured at $4° \pm 3°$ deg. In addition to fits to the logarithmic spiral equation, we also fitted the spiral trace to the general Archimedean equation. The result is shown in Appendix A. We note that because scattered light originate from a cone-shape surface instead of a flat plane, when viewed at a finite inclination, different regions in the disk are compressed differently (e.g., Fig. 4, Ginski et al. 2016). Because of this, a disk structure in surface density traced by mm continuum emission can be projected to a different location in scattered light (e.g., the southern spiral arm in MWC 758, Dong et al. 2018b). Simple deprojection by linearly expanding the disk along the minor axis by a factor of $1/\cos i$ generally does not perfectly restore the face-on view of the disk (Dong et al. 2016). Therefore, our measurements of the arm pitch angles are approximations only. Future modeling work is needed to simultaneously determine the shapes of the disk surface and the spiral arms.

We used both fit results to infer input parameters for the forward modeling of the $L'$-band feature (for the detailed method for the forward modeling, see Christiaens et al. 2019) to measure a throughput (signal loss due to the ADI reduction); Fig. 6 shows our result with injected spirals. We used the off-axis PSF of CQ Tau and injected several separations and position angles to produce fake spiral features (injected positions shown in Figure 6). We then measured the ratio between input flux and output flux at the injected locations, which is shown in the right image of Figure 6. Our forward modeling reproduced the outer spiral with a flux recovered by a throughput of 0.54 at 50 au, but the injected inner spiral is largely affected (a throughput less than 0.3) by not only self-subtraction at small separations but also negative regions produced by the existence of the outer spiral. As the SNRs of this feature in the practical NIRC2 and HiCIAO data are less than 5, we do not conclude that this inner feature is a spiral.

The CQ Tau disk has a striking similarity with the disk around V1247 — both of which show one prominent arm in scattered light and a ringed disk in mm continuum emission (Ohta et al. 2016; Kraus et al. 2017). In addition, they share a similar inclination of $\sim 30 - 35°$, and the major spiral arm seen is in the direction of the major axis. Simulations have shown that while a massive companion may induce a pair of nearly symmetric spiral arms, when viewed at a modest inclination one of the arms may be compressed more than the other in scattered light, thus falling inside the inner working angle (Dong et al. 2016). Future observations may push for inner separations to look for possible additional arms hidden under the current image mask.

## 3. DISCUSSION

[29]IRAF is distributed by National Optical Astronomy Observatory, which is operated by the Association of Universities for Research in Astronomy, Inc., under cooperative agreement with the National Science Foundation.

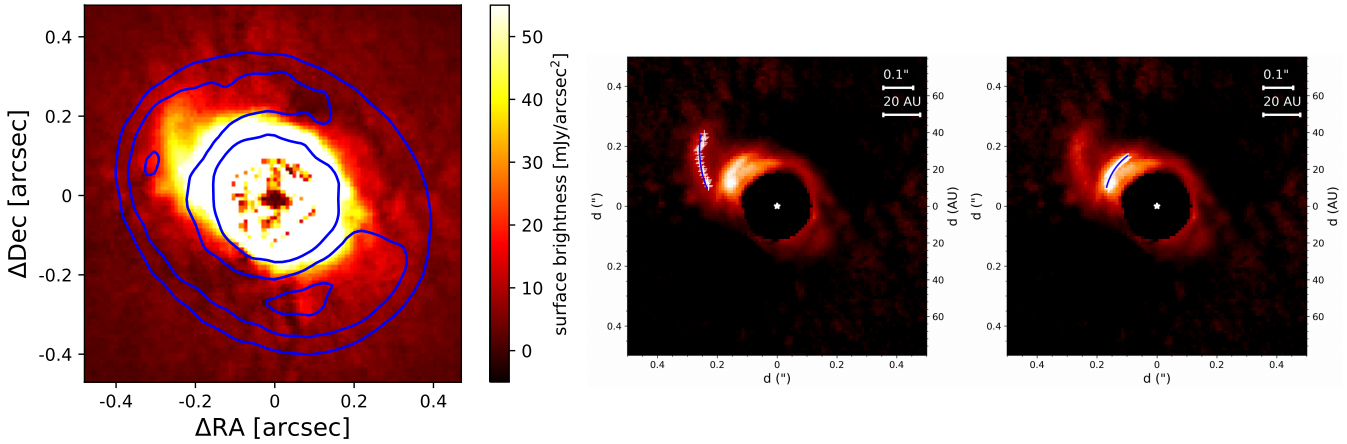


**Figure 4.** (left) PI image of Subaru/HiCIAO $H$-band observation overlaid with the ALMA continuum. North is up and east is left. (middle) $R^2$-scaled PI image including the identified trace of the outer spiral (white crosses) and the best-fit logarithmic spiral (blue curve). (right) Same for the inner (tentative) spiral. For estimating the pitch angle we used a further-deprojected image.

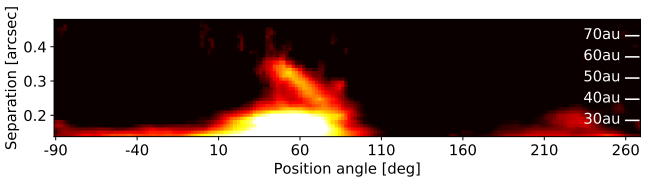


**Figure 5.** As Figure 2 for the $r^2$-scaled HiCIAO PI image.

The spiral feature in $L'$-band, the maximum brightness of which is 68 mJy/arcsec$^2$ with a throughput of 0.54 at 50 au, may be reproduced by two scenarios; 1) the surface of the spiral scatters the stellar light as shown in the Subaru/HiCIAO image 2) the spiral is heated and self-luminous. We consider two possibilities in this section to reproduce 126 mJy/arcsec$^2$ as the original spiral brightness.

### 3.1. *Scattering Case*

We first investigate whether the $L'$-band brightness can be reproduced by only scattering. As a rough estimate of the surface brightness of the scattered light, we use Equation (9) in Inoue et al. (2008), which is an approximate analytic expression of the scattered light (D'Alessio et al. 1999, 2006). We adopt $\Sigma_{\rm small}$=0.0375 g/cm$^2$ for the surface density of small dust (Ubeira Gabellini et al. 2019) and $\kappa\sim$100 cm$^2$/g (Birnstiel et al. 2018) at $H$- and $L'$-bands to estimate $\tau_\nu = \Sigma_{\rm small} \times \kappa$ at the spiral. Then $\tau_\nu$ is assessed as 3.75 and we assume an optically-thick disk. Finally, the observable intensity is given by a following equation

$$I_\nu^{\rm sca} \simeq \beta \omega_\nu H(1,\omega_\nu) B_\nu(T_\star) \frac{\Omega_\star}{4\pi} \cos(i) \ , \qquad (1)$$

where $\beta$, $\omega_\nu$, $\Omega_\star$, $T_\star$ and, $i$ are a grazing angle, albedo, a solid angle of the stellar photosphere from the spiral, effective temperature of CQ Tau, and inclination of the disk, respectively (for detailed explanations see Section 2 in Inoue et al. 2008). $H(1,\omega_\nu)$ represents the law of diffuse reflection (Chandrasekhar 1960) and $B_\nu(T_\star)$ is Planck's law. We also adopted assumptions for a typical disk as Inoue et al. (2008); $\beta = 0.05$ [rad], $\omega_\nu = 0.5$, $H(1,\omega_\nu) = 1$, $\Omega_\star = \frac{\pi}{2}\frac{R_\star^2}{r_{\rm spiral}^2}$. $R_\star$ was derived from Stefan-Boltzmann law with $T_\star$=6900 K and $L_\star = 10 L_\odot$ (Testi et al. 2001; Ubeira Gabellini et al. 2019). We used 50 au as a typical value for $r_{\rm spiral}$ and $i = 35°$ for the disk's inclination (Ubeira Gabellini et al. 2019). We finally assessed the expected scattered brightness as 18 and 5.0 mJy/arcsec$^2$ at $H$- and $L'$-band, respectively. Note that we do not take into account of polarization ratio for the HiCIAO data. In the HiCIAO result, the spiral has surface brightness of $\sim$30–40 mJy/arcsec$^2$ and does not show a large disagreement. If the spiral is flared like LkHa 330 (Uyama et al. 2018) the grazing angle can be larger and Equation (1) yields a good agreement with the HiCIAO result. The NIRC2 result, however, is much brighter than the expected brightness in $L'$-band even if the larger grazing angle is assumed. Therefore our $L'$-band result cannot be explained by only scattered light from the spiral surface.

### 3.2. *Hot Spiral Case*

Thermal emission from small grains may need to be included to explain the disk brightness in $L'$-band. Provided that small grains at the spiral absorb shorter wavelengths of stellar light and emit their heat at $\sim$3–4 $\mu$m, the grain temperature is given by the following equation

$$\begin{aligned}(1-\omega_\nu)\pi a_{\rm grain}^2 \frac{L_\star}{r_{\rm spiral}^2} &< Q_{\rm abs}(\lambda_\star) > \\ &= 4\pi a_{\rm grain}^2 \sigma T_{\rm grain}^4 Q_{\rm abs}(\lambda_{\rm grain}),\end{aligned} \qquad (2)$$

where $Q_{\rm abs}(\lambda)$ is the absorption efficiency at $\lambda$ and $a_{\rm grain}$ is the size of the grain. Assuming $< Q_{\rm abs}(\lambda_\star) > = \frac{\int Q_{\rm abs} B_\lambda(T_\star) d\lambda}{\int B_\lambda(T_\star) d\lambda} \simeq 1$ and an astronomical silicate model (Draine & Lee 1984), we find a set of $T_{\rm grain} \sim 202.5$ K and $a_{\rm grain} \sim 0.65$ $\mu$m can reproduce $I_\nu^{\rm emi} = 126$ mJy/arcsec$^2$. We investigated whether this $T_{\rm grain}$ is consistent with a flared spiral. We calculated the sound speed ($c_s$) and the Keplerian angular velocity ($\Omega_{\rm K}$) at 50 AU and 202.5 K, which is used to derive a scale height ($H = c_s/\Omega_{\rm K}$). The grazing angle is approximately $H/r_{\rm spiral} = 0.15$ and agrees with a flared spiral case. By reconsidering Equation (1) the expected scattered brightness at $H$-band turns into 54 mJy/arcsec$^2$, which can reproduce the ob-

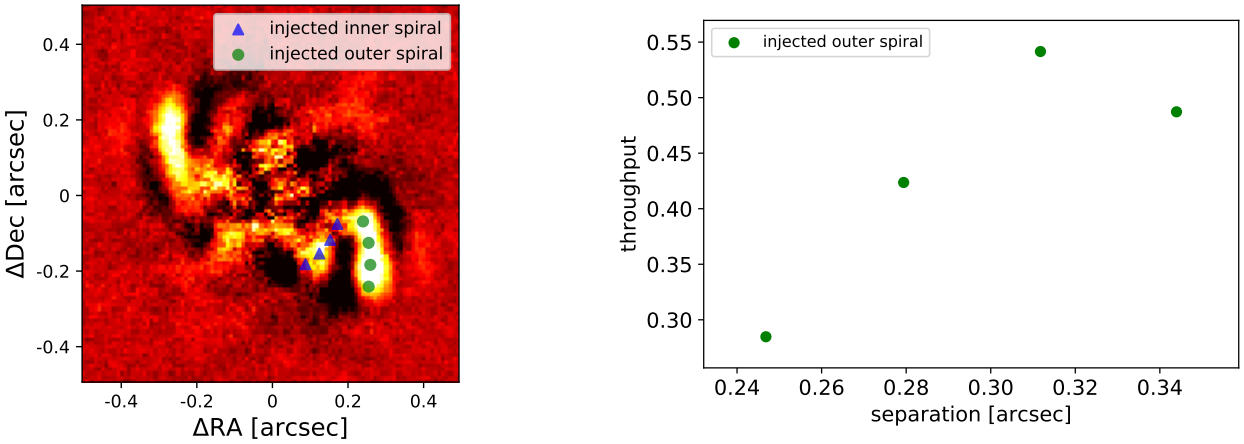


**Figure 6.** (left) VIP-PCA reduced image for the NIRC2 data with injected fake spirals at symmetric positions with respect to the center. (right) Measured throughput of the injected outer spiral as a function of separation.

served intensity in the $H$-band HiCIAO data with a certain polarization ratio.

This parameter $H/r_{\rm spiral}$ also approximately corresponds to the pitch angle induced by a small protoplanet (Rafikov 2002; Bae & Zhu 2018). However, the fitted result from the $r^2$-scaled HiCIAO image is much larger than the expected $H/r_{\rm spiral} \sim 0.15$. Several mechanisms can induce a large pitch angle: a gas giant ($\leq$15-20 deg; Zhu et al. 2015; Dong et al. 2015b), gravitational instability ($\leq$15–20 deg; Dong et al. 2015a), or shadow casting ($\leq$20–25 deg; Montesinos et al. 2016; Montesinos & Cuello 2018). Note that these studies basically assumed vertically isothermal disk temperature profile. Juhász & Rosotti (2018) performed another simulation by assuming the disk surface is hotter than the midplane and showed that the pitch angle can be more opened near the surface. As we mentioned in Section 2.2, our fitted result of the pitch angle ($34^\circ \pm 2^\circ$) can be distorted by the inclination effect and we do not identify the mechanism to open the spiral up. Combining gas observations of different emission lines enables to estimate the vertical temperature profile of the disk (Akiyama et al. 2011, 2013) and such future observations will help to understand the thermal structure of the spiral.

There are additional mechanisms that can make the spiral bright in $L'$-band and we investigate them hereafter. Currie et al. (2015) reported that HD 100546 also has an unexpectedly bright spiral in $L'$-band. To reproduce this feature Lyra et al. (2016) performed a 2D simulation and predicted that a high-mass planet can induce shocks and heats the spiral to a few hundred Kelvin (see Figure 4 in the paper). Although Hord et al. (2017) concluded that the HD 100546's spiral feature in $L'$-band can be reproduced by scattered light from its surface, the prediction of Ubeira Gabellini et al. (2019) of an unseen protoplanet is consistent with a heated spiral scenario. Since the NIRC2 observation did not detect any companion candidates, follow-up observations to search for planets within 30 AU are required to further investigate this scenario. The heating of the spiral arms driven by a massive companion is naturally expected due to shock heating (Zhu et al. 2015). We investigated the thermal energy of the predicted unseen protoplanet in Ubeira Gabellini et al. (2019). Given a 10-Myr and 10 $M_{\rm J}$ protoplanet its luminosity is expected $10^{-3.7}$ $L_\odot$ with COND03 model, which is $10^{-4.7}$ fainter than CQ Tau. Even if taking into account of the difference of separation to the spiral, the thermal energy of this possible planet may not be responsible for heating comparable to that by the central star.

Current data do not allow us to resolve the degeneracy between these different heating sources. Follow-up observations for the disk exploration as well as the companion search will help to understand this bright spiral feature. The $L'$-band profile for the spiral feature may be improved by high-contrast imaging with RDI. Also, PDI observations with an updated AO instrument such as Subaru/SCExAO, Gemini/GPI, or VLT/SPHERE will be able to provide a clearer image of the disk.

Some of the data presented herein were obtained at the W. M. Keck Observatory, which is operated as a scientific partnership among the California Institute of Technology, the University of California and the National Aeronautics and Space Administration. The Observatory was made possible by the generous financial support of the W. M. Keck Foundation. A part of this research is based on data collected at the Subaru Telescope, which is operated by the National Astronomical Observatories of Japan. Based in part on data collected at Subaru telescope and obtained from the SMOKA, which is operated by the Astronomy Data Center, National Astronomical Observatory of Japan. This research has made use of NASA's Astrophysics Data System Bibliographic Services. This research has made use of the SIMBAD database, operated at CDS, Strasbourg, France. This research has made use of the VizieR catalogue access tool, CDS, Strasbourg, France. The original description of the VizieR service was published in A&AS 143, 23.

TU acknowledges JSPS overseas research fellowship. This work was supported by MEXT/JSPS KAKENHI Grant Numbers 15H02063, 17K05399, 18H05442, 19H00703, 19H05089, and 19K03932. Part of this work was carried out at the Jet Propulsion Laboratory, California Institute of Technology, under contract with the National Aeronautics and Space Administration (NASA). VC acknowledges funding from the Australian Research Council via DP180104235.

The authors wish to acknowledge the very significant cultural role and reverence that the summit of Mauna Kea has always had within the indigenous Hawaiian community. We are most fortunate to have the opportunity to conduct observations from this mountain.

## REFERENCES


Akiyama, E., Momose, M., Hayashi, H., & Kitamura, Y. 2011, PASJ, 63, 1059, doi: 10.1093/pasj/63.5.1059

Akiyama, E., Momose, M., Kitamura, Y., et al. 2013, PASJ, 65, 123, doi: 10.1093/pasj/65.6.123

ALMA Partnership, Brogan, C. L., Pérez, L. M., et al. 2015, ApJ, 808, L3, doi: 10.1088/2041-8205/808/1/L3

Amara, A., & Quanz, S. P. 2012, Monthly Notices of the Royal Astronomical Society, 427, 948, doi: 10.1111/j.1365-2966.2012.21918.x

Bae, J., & Zhu, Z. 2018, ApJ, 859, 119, doi: 10.3847/1538-4357/aabf93

Baraffe, I., Chabrier, G., Barman, T. S., Allard, F., & Hauschildt, P. H. 2003, A&A, 402, 701, doi: 10.1051/0004-6361:20030252

Benisty, M., Juhasz, A., Boccaletti, A., et al. 2015, A&A, 578, L6, doi: 10.1051/0004-6361/201526011

Birnstiel, T., Dullemond, C. P., Zhu, Z., et al. 2018, ApJ, 869, L45, doi: 10.3847/2041-8213/aaf743

Chandrasekhar, S. 1960, Radiative transfer

Chapillon, E., Parise, B., Guilloteau, S., Dutrey, A., & Wakelam, V. 2010, A&A, 520, A61, doi: 10.1051/0004-6361/201014841

Christiaens, V., Casassus, S., Absil, O., et al. 2019, MNRAS, 486, 5819, doi: 10.1093/mnras/stz1232

Currie, T., Cloutier, R., Brittain, S., et al. 2015, ApJ, 814, L27, doi: 10.1088/2041-8205/814/2/L27

D'Alessio, P., Calvet, N., Hartmann, L., Franco-Hernández, R., & Servín, H. 2006, ApJ, 638, 314, doi: 10.1086/498861

D'Alessio, P., Calvet, N., Hartmann, L., Lizano, S., & Cantó, J. 1999, ApJ, 527, 893, doi: 10.1086/308103

Dong, R., Fung, J., & Chiang, E. 2016, ApJ, 826, 75, doi: 10.3847/0004-637X/826/1/75

Dong, R., Hall, C., Rice, K., & Chiang, E. 2015a, ApJ, 812, L32, doi: 10.1088/2041-8205/812/2/L32

Dong, R., Najita, J. R., & Brittain, S. 2018a, ApJ, 862, 103, doi: 10.3847/1538-4357/aaccfc

Dong, R., Zhu, Z., Rafikov, R. R., & Stone, J. M. 2015b, ApJ, 809, L5, doi: 10.1088/2041-8205/809/1/L5

Dong, R., Liu, S.-y., Eisner, J., et al. 2018b, ApJ, 860, 124, doi: 10.3847/1538-4357/aac6cb

Draine, B. T., & Lee, H. M. 1984, ApJ, 285, 89, doi: 10.1086/162480

Gaia Collaboration, Brown, A. G. A., Vallenari, A., et al. 2018, A&A, 616, A1, doi: 10.1051/0004-6361/201833051

Ginski, C., Stolker, T., Pinilla, P., et al. 2016, A&A, 595, A112, doi: 10.1051/0004-6361/201629265

Gomez Gonzalez, C. A., Wertz, O., Absil, O., et al. 2017, AJ, 154, 7, doi: 10.3847/1538-3881/aa73d7

Hashimoto, J., Tamura, M., Muto, T., et al. 2011, ApJ, 729, L17, doi: 10.1088/2041-8205/729/2/L17

Hashimoto, J., Dong, R., Kudo, T., et al. 2012, ApJ, 758, L19, doi: 10.1088/2041-8205/758/1/L19

Hord, B., Lyra, W., Flock, M., Turner, N. J., & Mac Low, M.-M. 2017, ApJ, 849, 164, doi: 10.3847/1538-4357/aa8fcf

Inoue, A. K., Honda, M., Nakamoto, T., & Oka, A. 2008, PASJ, 60, 557, doi: 10.1093/pasj/60.3.557

Juhász, A., & Rosotti, G. P. 2018, MNRAS, 474, L32, doi: 10.1093/mnrasl/slx182

Keppler, M., Benisty, M., Müller, A., et al. 2018, A&A, 617, A44, doi: 10.1051/0004-6361/201832957

Kraus, S., Kreplin, A., Fukugawa, M., et al. 2017, ApJ, 848, L11, doi: 10.3847/2041-8213/aa8edc

Kuhn, J. R., Potter, D., & Parise, B. 2001, ApJ, 553, L189, doi: 10.1086/320686

Lyra, W., Richert, A. J. W., Boley, A., et al. 2016, ApJ, 817, 102, doi: 10.3847/0004-637X/817/2/102

Marois, C., Macintosh, B., Barman, T., et al. 2008, Science, 322, 1348, doi: 10.1126/science.1166585

Mawet, D., Choquet, É., Absil, O., et al. 2017, AJ, 153, 44, doi: 10.3847/1538-3881/153/1/44

McDonald, I., Zijlstra, A. A., & Watson, R. A. 2017, Monthly Notices of the Royal Astronomical Society, 471, 770, doi: 10.1093/mnras/stx1433

Milli, J., Mouillet, D., Lagrange, A. M., et al. 2012, A&A, 545, A111, doi: 10.1051/0004-6361/201219687

Montesinos, M., & Cuello, N. 2018, MNRAS, 475, L35, doi: 10.1093/mnrasl/sly001

Montesinos, M., Perez, S., Casassus, S., et al. 2016, ApJ, 823, L8, doi: 10.3847/2041-8205/823/1/L8

Muto, T., Grady, C. A., Hashimoto, J., et al. 2012, ApJ, 748, L22, doi: 10.1088/2041-8205/748/2/L22

Natta, A., Prusti, T., Neri, R., et al. 2001, A&A, 371, 186, doi: 10.1051/0004-6361:20010334

Ohta, Y., Fukagawa, M., Sitko, M. L., et al. 2016, PASJ, 68, 53, doi: 10.1093/pasj/psw051

Pérez, L. M., Carpenter, J. M., Andrews, S. M., et al. 2016, Science, 353, 1519, doi: 10.1126/science.aaf8296

Pinte, C., Price, D. J., Ménard, F., et al. 2018, ApJ, 860, L13, doi: 10.3847/2041-8213/aac6dc

Rafikov, R. R. 2002, ApJ, 569, 997, doi: 10.1086/339399

Reggiani, M., Christiaens, V., Absil, O., et al. 2018, A&A, 611, A74, doi: 10.1051/0004-6361/201732016

Ruane, G., Ngo, H., Mawet, D., et al. 2019, AJ, 157, 118, doi: 10.3847/1538-3881/aafee2

Serabyn, E., Huby, E., Matthews, K., et al. 2017, AJ, 153, 43, doi: 10.3847/1538-3881/153/1/43

Soummer, R., Pueyo, L., & Larkin, J. 2012, The Astrophysical Journal, 755, L28, doi: 10.1088/2041-8205/755/2/L28

Strom, K. M., Strom, S. E., Edwards, S., Cabrit, S., & Skrutskie, M. F. 1989, AJ, 97, 1451, doi: 10.1086/115085

Tamura, M. 2009, in American Institute of Physics Conference Series, ed. T. Usuda, M. Tamura, & M. Ishii, Vol. 1158, 11–16, doi: 10.1063/1.3215811

Tang, Y.-W., Guilloteau, S., Dutrey, A., et al. 2017, ApJ, 840, 32, doi: 10.3847/1538-4357/aa6af7

Testi, L., Natta, A., Shepherd, D. S., & Wilner, D. J. 2001, ApJ, 554, 1087, doi: 10.1086/321406

Ubeira Gabellini, M. G., Miotello, A., Facchini, S., et al. 2019, MNRAS, 486, 4638, doi: 10.1093/mnras/stz1138

Uyama, T., Hashimoto, J., Kuzuhara, M., et al. 2017, AJ, 153, 106, doi: 10.3847/1538-3881/153/3/106

Uyama, T., Hashimoto, J., Muto, T., et al. 2018, AJ, 156, 63, doi: 10.3847/1538-3881/aacbd1

van der Marel, N., van Dishoeck, E. F., Bruderer, S., et al. 2013, Science, 340, 1199, doi: 10.1126/science.1236770

Wagner, K., Stone, J. M., Spalding, E., et al. 2019, arXiv e-prints, arXiv:1907.06655. https://arxiv.org/abs/1907.06655

Xuan, W. J., Mawet, D., Ngo, H., et al. 2018, AJ, 156, 156, doi: 10.3847/1538-3881/aadae6

Zhu, Z., Dong, R., Stone, J. M., & Rafikov, R. R. 2015, ApJ, 813, 88, doi: 10.1088/0004-637X/813/2/88


## APPENDIX

### SUPPLEMENTARY KECK/NIRC2 IMAGES

We present supplementary images to clearly show our Keck/NIRC2 result. Figure 7 presents a set of different PCs. Figure 8 shows the NIRC2 results superimposed with the ALMA continuum (left) and a full FoV version of the VIP-ADI reduction (right). Figure 9 shows the best-fit Archimedean spirals ($r = a + b \times \theta^n$) that reproduce well the observed features (left for the outer spiral: $a = 0\farcs221 \pm 0\farcs004$, $b = 0\farcs203 \pm 0\farcs010$, $n = 0.744 \pm 0.045$ and right for the inner feature: $a = 0\farcs141 \pm 0\farcs006$, $b = 0\farcs056 \pm 0\farcs007$, $n = 0.149 \pm 0.079$).

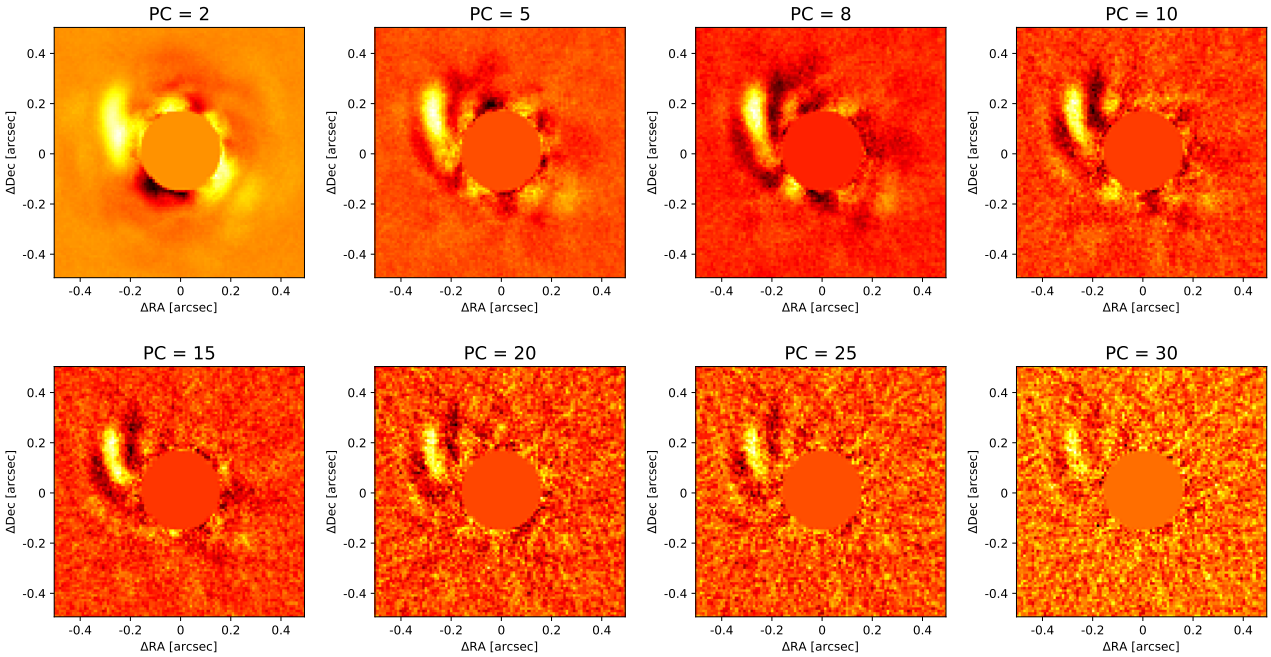


**Figure 7.** Keck/NIRC2 ADI-reduced images of CQ Tau at different PCs. These images also detected the same spiral structure with SNRs>5.

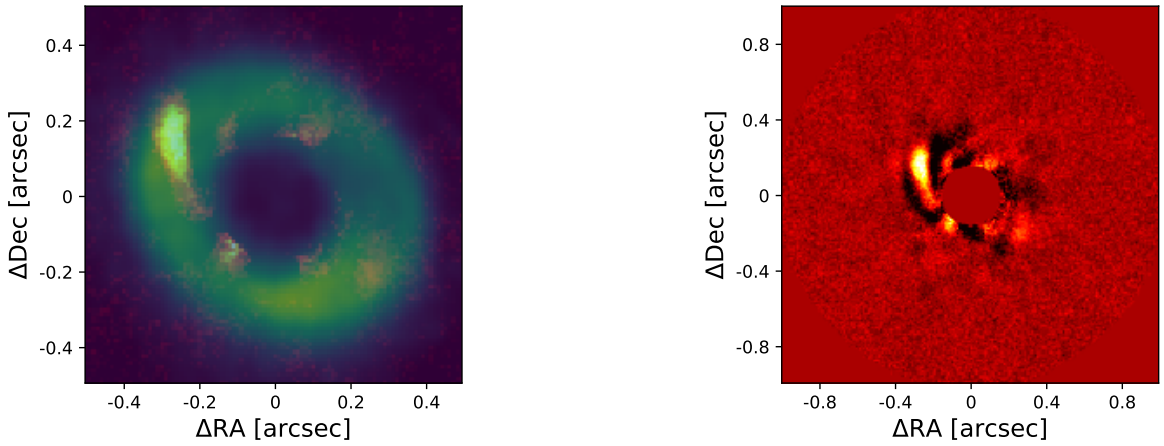


**Figure 8.** (left) As Figure 1 superimposed with the ALMA continuum (yellow-green). (right) ADI-reduced NIRC2 image (PC=8) with a larger FoV.

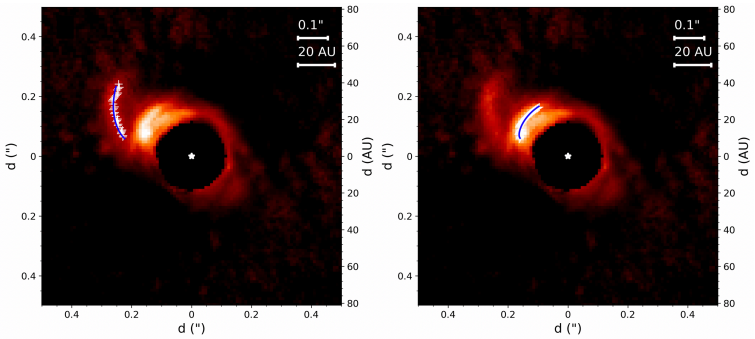


**Figure 9.** As middle and right images in Figure 4 for the fitted result with the best-fit general Archimedean spirals.